Corrosive degradation of a dense Si_3N_4 in a burner rig

T. GRAZIANI*, D. BAXTER
CEC-JRC, Institute for Advanced Materials, Petten, The Netherlands
A. BELLOSI
CNR-IRTEC, Faenza, Italy

The demands for greater efficiency and reduced environmental pollution are two of the main factors behind the intense research and development for new and improved materials for propulsion and power generation systems. On the grounds of density and retention of properties at high temperatures, ceramics are attractive alternatives to metallic materials. While much attention is focused on the problem of mechanical reliability, the question of corrosion resistance, and more importantly the synergism between corrosion and strength, are critical factors affecting the life of components. This investigation addresses the corrosion of a Si_3N_4, hot-pressed with 3% Al_2O_3 and 8% Y_2O_3, in a combustion atmosphere paying particular attention to corrosion. The results show that the dominant surface reaction in an atmosphere containing SO_2 and compounds of sodium was oxidation, giving a surface product of silica, but the kinetics were in some cases not parabolic as often reported. It was also shown that strength progressively decreased with increasing corrosion test temperature, probably due to the formation of subsurface defects.

1. Introduction

Good corrosion resistance and mechanical properties of SiC and Si_3N_4 advanced ceramics and their composites provide many advantages over metallic alloys in high temperature applications such as gas turbines and heat exchangers. Silicon nitride-based materials, for example, exhibit high resistance to oxidation up to 1400 °C, compared with less than 1000 °C for most metallic alloys. Increased engine operating temperatures makes more efficient fuel combustion possible with the consequent benefit of improved fuel economy and reduced environmental pollution. While numerous factors may contribute to material degradation, such as mechanical stress and particulate erosion, successful application of any non-oxide ceramic for long times at high temperatures in complex process atmospheres demands a good understanding of corrosion behaviour.

Burner rigs are useful at simulating the dynamic conditions of combustion environments (e.g. gas turbines), particularly compared with traditional crucible or furnace test procedures [1]. In general, the rate of corrosive degradation in gas turbine atmospheres can be related to the concentrations of contaminants in the fuel and ingested air, which together contribute to the formation of SO_2/SO_3 and $Na_2SO_4/Na_2O/NaCl$ in the gas stream. In a multiphase ceramic like fully dense Si_3N_4, corrosion in combustion environments can often proceed in a manner similar to that for oxidation with the formation of a silica layer. However, since SiO_2 is an acidic material, corrosion can be strongly promoted by alkaline conditions [2]. Thus the concentrations of SO_3 and Na_2O are important in determining observed rates of corrosion. Some of the reactions to be considered in a combustion gas are as follows:

$$Si_3N_4 + 3O_2(g) = SiO_2(s) + 2N_2(g) \quad (1)$$

$$2NaCl + SO_2 + 1/2\,O_2 + H_2O = Na_2SO_4 + 2HCl \quad (2)$$

$$Na_2SO_4 + xSiO_2(s) = Na_2O + xSiO_2(l) + SO_3(g) \quad (3)$$

$$2SiO_2 + Na_2O = Na_2Si_2O_5 \quad (4)$$

$$2SiO_2 + 2NaOH = Na_2Si_2O_5 + H_2O \quad (5)$$

Incorporation of sodium into the silica network leads to its breakdown [3], resulting in reduced viscosity and therefore in reduced protection capacity.

The outward diffusion of cations from the grain boundary phase is one of the suggested mechanisms providing the rate limiting step in the oxidation of hot-pressed Si_3N_4 in air [4, 5]. Grain boundaries, in which numerous defects are incorporated, are zones that permit relatively easy transport of species involved in corrosion reactions. The tailoring of high quality silicon nitride-based materials for attractive

* Present address: ISRIM, Terni, Italy.

0022–2461

mechanical properties must therefore take good account of the corrosion behaviour of the grain boundaries. Factors to be considered include purity of the starting powders, type and amounts of the sintering aids and the degree of crystallization of the grain boundary material. This work reports on the corrosion behaviour of a hot-pressed Si_3N_4–3 wt % Al_2O_3–8 wt % Y_2O_3 composition in terms of kinetics, microstructural changes and mechanical degradation after exposure to thermal cycles in a low-velocity burner rig in the temperature range 1000–1300 °C.

2. Experimental procedure

The material used in this work was a fully dense Si_3N_4 containing Al_2O_3 (3 wt %) and Y_2O_3 (8 wt %) produced by hot pressing. Preparation, mixing of the starting powders, sintering conditions and properties of this material are given elsewhere [6]. Test specimens were cut in the form of four-point bend bars 3 mm × 3 mm × 30 mm with the faces ground to a surface roughness of 0.2 μm and the edges chamfered. The bars were exposed to a combustion environment at 1.013×10^5 Pa pressure in a low velocity burner rig (gas velocity of 0.2 m s^{-1}). The experimental procedure was based on the VAMAS guidelines for hot-salt corrosion testing of superalloys [7]. The corrosion atmosphere was produced by burning a 1 wt % sulfur marine grade diesel fuel atomized with 1300 L h^{-1} of air (air-to-fuel ratio of 28:1 by weight) giving an equivalent SO_2 input of 310 p.p.m. To this was added an aqueous solution of artificial ocean water, made to ASTM D1141 standard, giving a total input of 13 mg cm^{-2} h^{-1} Na_2SO_4 (equivalent to 4 mg cm^{-2} h^{-1} of Na) from a composition with solid constituents in the proportions 59% NaCl, 10% Na_2SO_4, 26% $MgCl_2 \cdot 6H_2O$, 3% $CaCl_2$ and 1.7% KCl. Using the Solgasmix computer program the equilibrium composition was calculated [8]. Fig. 1 shows the calculated partial pressures of NaOH, SO_2 and SO_3 and the mole fraction of Na_2SO_4 in the combustion gases.

Experiments were carried out at temperatures of 1000, 1100, 1200 and 1300 °C, each for a total time of 50 h accumulated over eight short isothermal exposures of $6\frac{1}{4}$ h. After each $6\frac{1}{4}$ h cycle, the specimens (eight per temperature) were cooled freely in air and weighed. The simultaneous exposure of pure alumina rods (considered inert) showed that negligible deposition took place, thus indicating that at all temperatures all combustion products were gaseous. Kinetic data was also obtained by exposing the ceramic to an air–1 vol % SO_2 gas in a sensitive continuously recording thermobalance at temperatures of 1200 and 1300 °C. Microstructural investigations on outer surfaces, polished cross-sections and fracture surfaces of the Si_3N_4 test material were carried out by scanning electron microscopy (SEM) and microprobe techniques after non-destructive analysis by X-ray diffraction.

The flexural strength, for untreated and treated bars [9], both at room and high temperature, was measured on 3 × 3 × 30 mm specimens in a four-point bending fixture, with outer and inner spans of 26 and 13 mm, respectively, and a crosshead speed of 0.5 mm min^{-1}. For the high temperature tests, the set temperature was held for 10 min before loading in order to ensure thermal equilibrium. Since the evaluation of the flexural strength was based on the measurements of only four test pieces for each

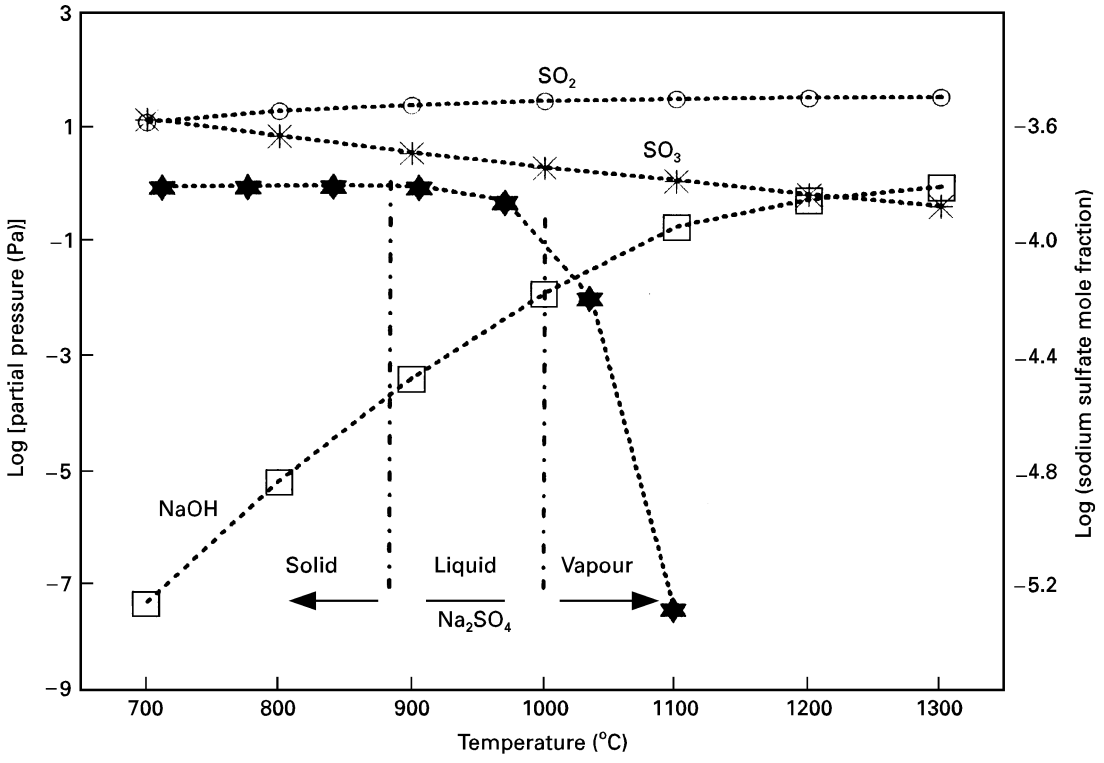

Figure 1 Concentrations of the main combustion products formed in the burner rig. Input species (by volume): SO_2 0.0003; H_2O 0.028; CH_4 0.033; O_2 0.188; N_2 0.751; NaCl 0.0001.

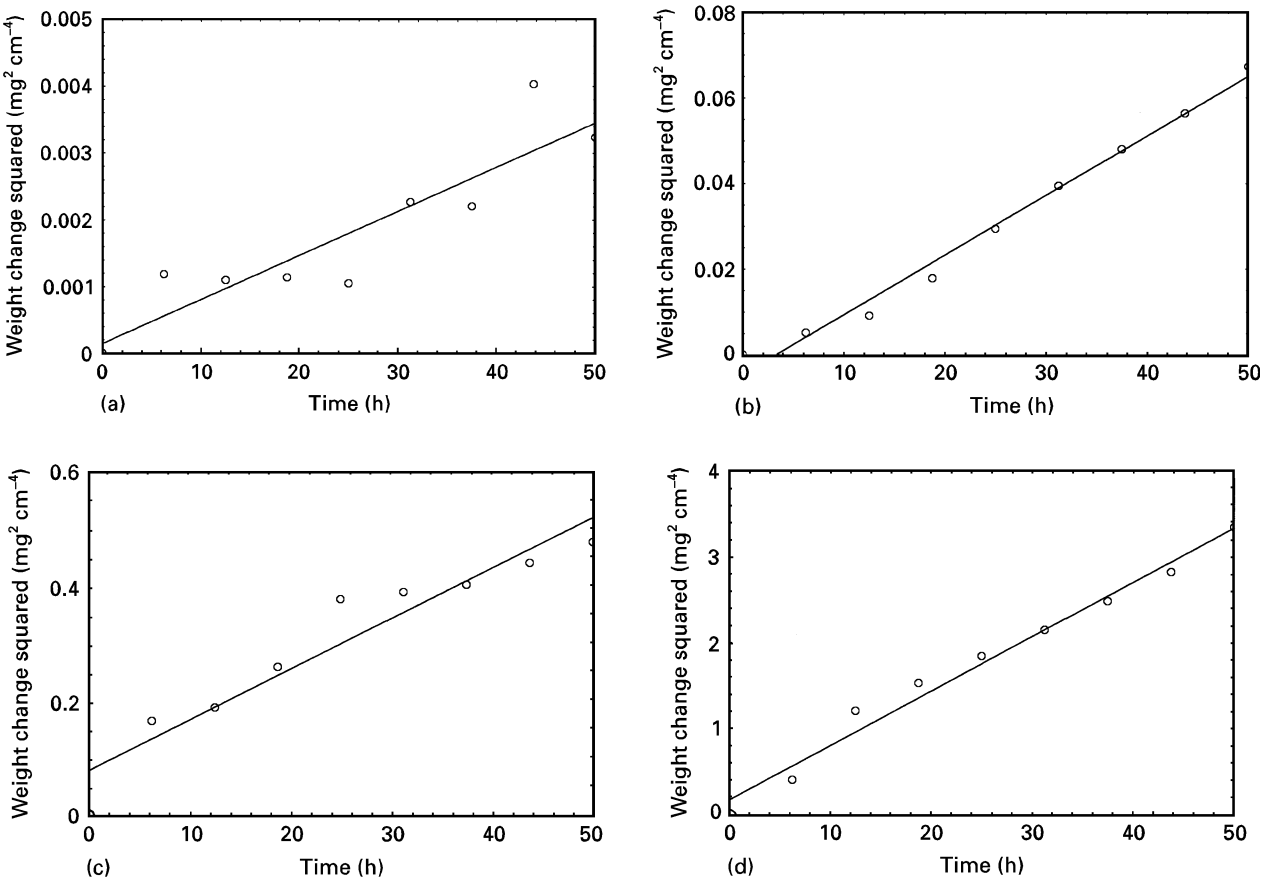

Figure 2 Weight change squared versus time plots of the ceramic exposed to the burner rig combustion gas for 50 h, showing determination of the parabolic rate constants. (a) 1000 °C, $y = (6.62 \times 10^{-5})x + 1.45 \times 10^{-4}$, $r^2 = 0.820$. (b) 1100 °C, $y = 0.00139x - 0.00455$, $r^2 = 0.988$, (c) 1200 °C, $y = 0.00871x + 0.0824$, $r^2 = 0.909$ and (d) 1300 °C, $y = 0.0637x + 0.160$, $r^2 = 0.983$.

temperature, room temperature and 1000 °C, caution must be exercised in the interpretation of the results.

3. Results

3.1. Kinetics

Weight change results for the Si_3N_4 ceramic corrosion tested in the temperature range 1000 to 1300 °C are shown in Fig. 2. Using the traditional approach of plotting the data in a weight change squared versus time format enables parabolic rate constants to be determined since:

$$(\Delta W/S)^2 = kt + c \tag{6}$$

where $(\Delta W/S)^2$ is weight gain squared, t is time, $k = k_0 \exp(-Q/RT)$ is the parabolic rate constant, Q is the apparent activation energy, R is the gas constant, T is the temperature and c is a constant accounting for weight gained during the initial, transient stages of the corrosion process. Taking the next step of plotting the parabolic rate constants in an Arrhenius diagram (Fig. 3) allowed an apparent activation energy of 387 kJ mol^{-1} to be calculated. For material of the same composition, an apparent activation energy of 630 kJ mol^{-1} has been reported for oxidation in air in the temperature range 1200 to 1400 °C [10]. In the latter case, the oxidation rate constants were lower ($\sim$2 orders of magnitude at 1200 °C) than those observed for corrosion in the burner rig.

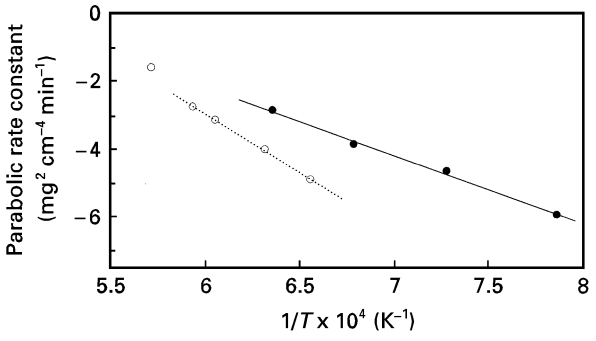

Figure 3 Arrhenius plot of the corrosion rates as a function of temperature (burner rig –●–; air –○– [10]).

The poor fit to true parabolic kinetics at some temperatures promoted an alternative analysis of the weight change data using a method adopted by Nickel [11] from a procedure originally proposed by Deal and Groves [12]. The method recognizes the contributions of reactions giving linear and logarithmic as well as parabolic kinetics either individually or in combination. The method therefore uses a starting equation of the general form;

$$w = at + bt^{0.5} + c\log(t) \tag{7}$$

and by multiple linear regression arrives at a solution for the constants a, b and c. (Note: In cases where a negative value for a constant was obtained, the regression analysis was repeated, but only with

components with positive constants from the first attempt.) The resulting best fit equations for the weight data are as follows (t in hours):

$$1000\,^{\circ}\mathrm{C}\quad w = 4\times10^{-3} + (7.6\times10^{-3})t^{0.5}\quad (R = 0.007) \tag{8}$$

$$1100\,^{\circ}\mathrm{C}\quad w = 1.8\times10^{-3} + (3.8\times10^{-2})t^{0.5}\quad (R = 0.007) \tag{9}$$

$$1200\,^{\circ}\mathrm{C}\quad w = (2.8\times10^{-2})t + 0.4\log(t)\quad (R = 0.04) \tag{10}$$

$$1300\,^{\circ}\mathrm{C}\quad w = (7\times10^{-3})t + 0.8\log(t)\quad (R = 0.06) \tag{11}$$

$$(\text{or } 0.14\,t^{0.5} + 0.47\log(t)\quad (R = 0.06)$$

where R is standard deviation.

While the small number of data points at each temperature limits confidence in very accurate interpretation of the kinetics, it is nevertheless important to note that there appears to be a significant non-parabolic contribution to the corrosion kinetics at 1200 °C and above. Increasing the amount of weight change data in relatively short term burner rig tests is not practical, so additional kinetic data was obtained from thermobalance tests in air + 1 vol % SO_2 at 1200 and 1300 °C in order to permit further analysis of the rates of corrosion. The weight change curves, each obtained from more than 2000 measuring points, are shown in Fig. 4. Again, the rates most closely follow a logarithmic relationship, rather than parabolic.

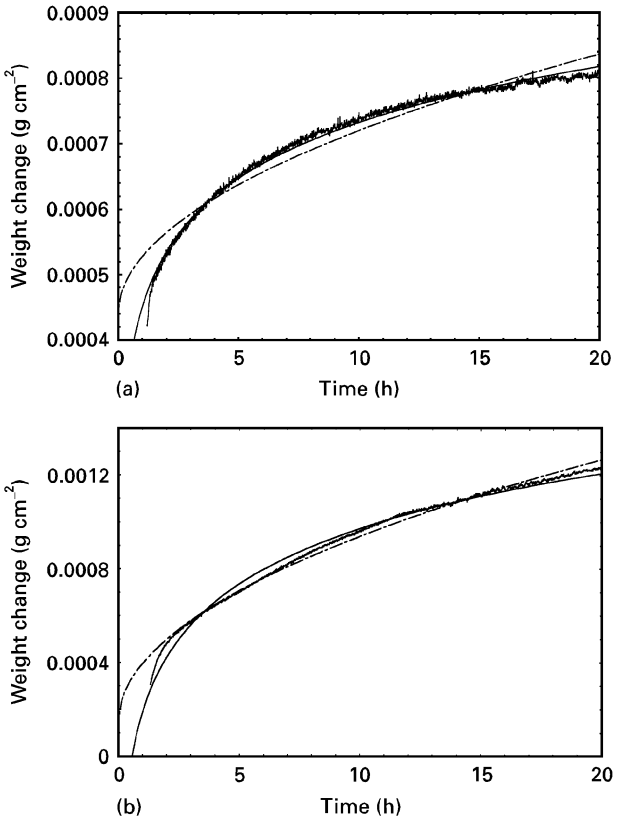

Figure 4 Weight change data obtained from thermobalance tests in air +1 vol % SO_2 at (a) 1200 (—$y = 4.5\times10^{-4} + 2.8\times10^{-4}\log(x)$, $R = 6.87\times10^{-6}$; – · – · –$y = 4.4\times10^{-4} + 8.9\times10^{-5}\,x^{0.5}$, $R = 2.04\times10^{-5}$) (b) 1300 °C ($-\,y = 1.8\times10^{-4} + 7.9\times10^{-4}\log(x)$, $R = 2.27\times10^{-5}$; – · – · –$y = 1.4\times10^{-4} + 2.5\times10^{-4}\,x^{0.5}$ $R = 2.09\times10^{-5}$).

3.2. Microstructural change

X-ray diffraction analysis confirmed the presence of silica in the form of cristobalite as the major constituent of the corrosion layer in the burner rig tested material, increasing in amount with temperature up to 1200 °C, but not increasing further at 1300 °C (Fig. 5). The only other crystalline phase detected was yttrium disilicate ($Y_2Si_2O_7$), whose proportion was independent of temperature up to 1200 °C, thereafter increasing only slightly (Fig. 5). In addition to the formation of a surface scale, devitrification of the grain boundary phase, due to the heat treatment, was also observed.

The SEM and energy dispersive spectroscopy (EDX) examinations on external surfaces and fracture surfaces confirmed the phases detected by X-ray diffraction as well as the presence of a continuous glassy scale. At 1000 °C, small protrusions associated with porosity in the corrosion product were aligned along grinding marks on the ceramic surface (Fig. 6a). EDX analysis of the protrusions gave Si as the main constituent, with small traces of Al which had diffused out from the grain boundary phase in the base ceramic. Elsewhere in the 5 μm thick scale (Fig. 6b), EDX showed the presence of Al, Y, Na, Ca, K and Cl in the glassy layer. Examination of fracture sections revealed high concentrations of Al, S, Cl, K and Ca at the interface between the corrosion layer and the bulk ceramic. The thickness of the scale was 10 μm at 1100 °C with comparatively more protrusions and porosity in the outer scale surface and a change in morphology of the $Y_2Si_2O_7$ phase to a more compact form (Fig. 7). Cracking of the glassy layer during cooling caused fracture of the $Y_2Si_2O_7$ particles (Fig. 8). The distribution of $Y_2Si_2O_7$ in the thickness of the surface scale is shown in Fig. 9 along with voids associated with the evolution of nitrogen. Scale thickness increased to 25 μm at 1200 °C and 50–80 μm at 1300 °C. Voiding was most pronounced after exposure at 1300 °C (Fig. 10).

3.3. Hot corrosion effect on the strength

The flexural strength values of the ceramic measured at different temperatures on the as received material and after the burner rig tests are reported in Table I.

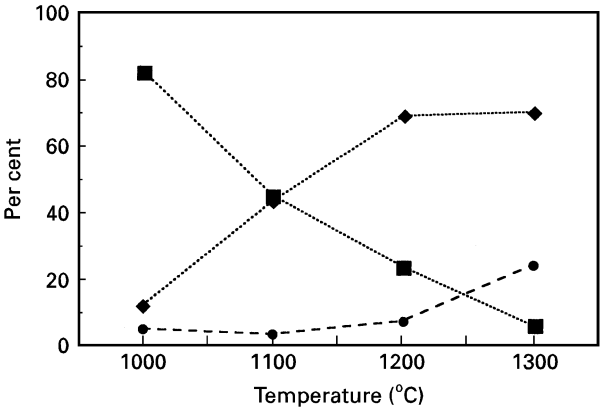

Figure 5 Concentration (%) of crystalline phases detected by X-ray diffraction on burner rig exposed surfaces (···■··· base material; ····◆···· SiO_2; ––●–– $Y_2Si_2O_7$).

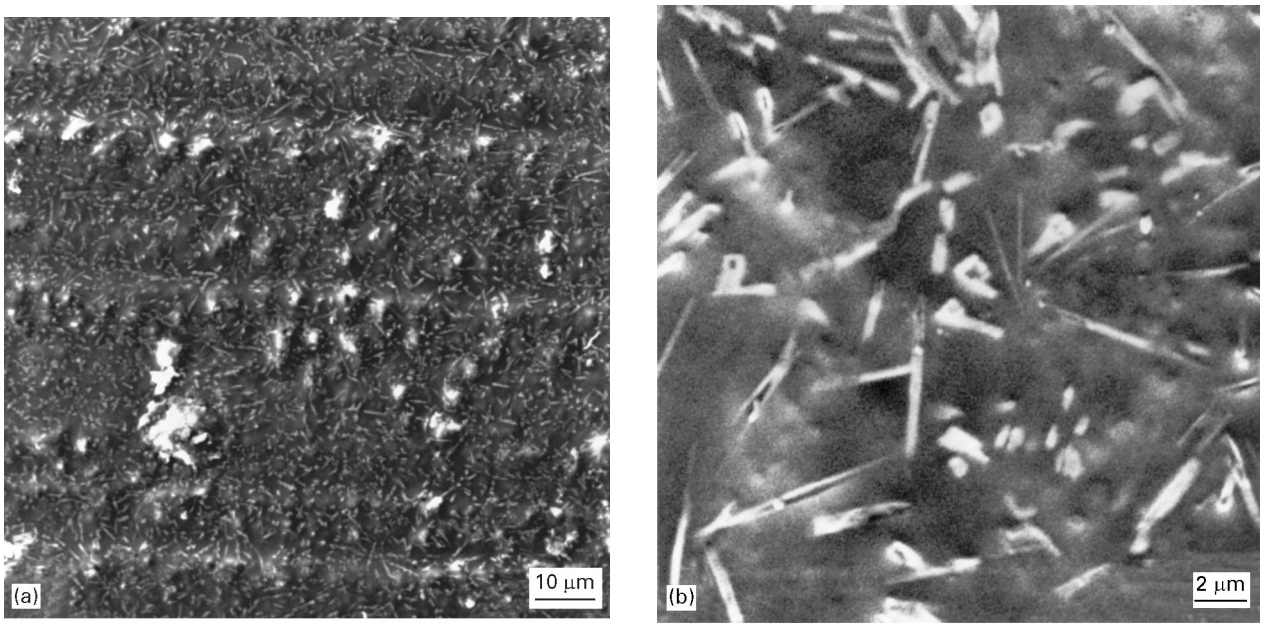

Figure 6 SEM micrographs of (a) surface protrusions and (b) SiO_2–$Y_2Si_2O_7$–glassy scale at 1000 °C.

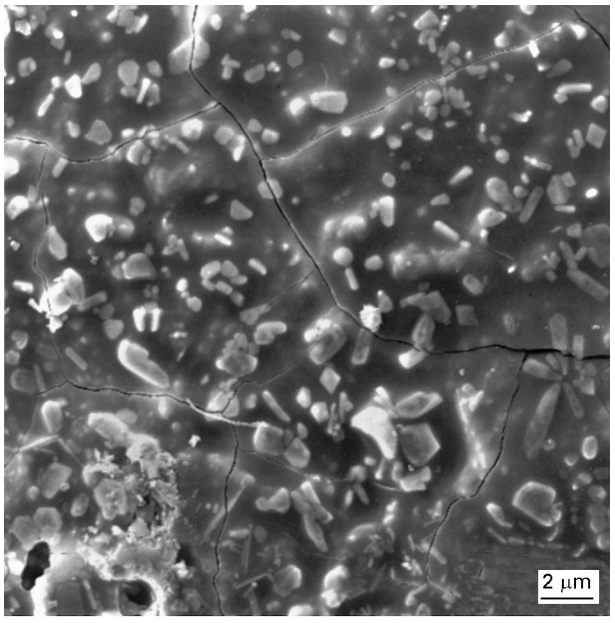

Figure 7 SEM micrograph showing the distribution and the morphology of $Y_2Si_2O_7$ crystals (1100 °C).

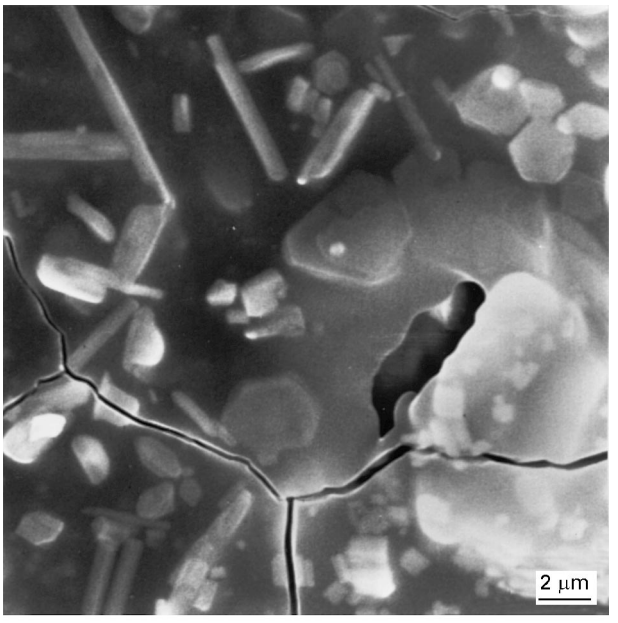

Figure 8 SEM micrograph of the cracked glass on the surface of the material treated at 1100 °C.

From the data, it would appear that a decrease in room temperature strength of ~33% to ~56% was produced by corrosion exposures in the range 1000–1300 °C (Fig. 11). The strength of the as-received material at 1000 °C is indeed ~37% less than that measured at room temperature (Fig. 12), indicating the high temperature of the mechanical test can also cause softening of any glassy intergranular phase. No variation was detected in strength measured at room temperature and at 1000 °C on samples corroded at 1300 °C for 50 h.

4. Discussion

Numerous studies have addressed the oxidation/corrosion mechanisms of Si_3N_4-based materials and several mechanisms to account for observed behaviour have been proposed. However, full understanding of the corrosion processes of these materials is still to be achieved. While for many years parabolic or near parabolic kinetics have usually been reported, different mechanistic models accounting for diffusion rate control have been proposed and include: (a) diffusion of oxygen through the oxide scale; (b) diffusion of cations through the grain boundary phases towards the reaction interface [4, 5]; and (c) outward diffusion of SiO_2 in the surface melt [13].

In many cases, Si_3N_4-based materials actually display more complex kinetic behaviour with corrosion rates changing as a function of temperature and time [11]. This was certainly the case in this work as shown by the relationships in Equations 8 to 11 and in Fig. 4.

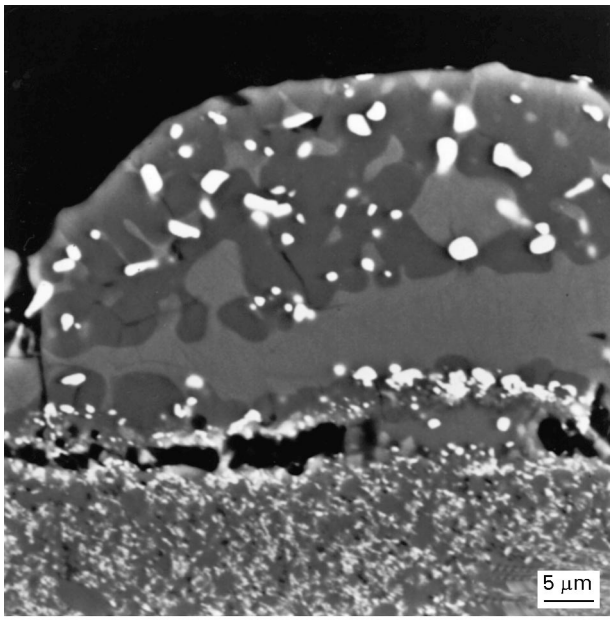

Figure 9 BSE micrographs showing the distribution of $Y_2Si_2O_7$ (white crystals) and voids in the scale of the sample treated at 1200 °C.

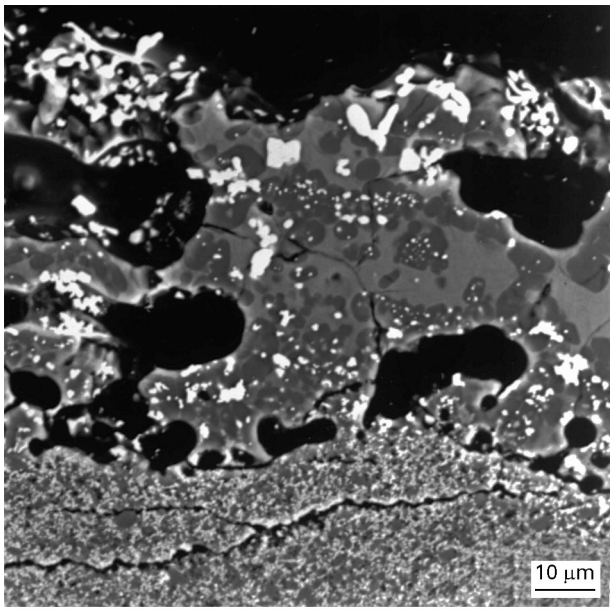

Figure 10 BSE micrographs of the cross-section showing voiding in the scale formed at 1300 °C.

TABLE I Flexural strength (MPa)[a]

Si_3N_4–3 wt % Al_2O_3–8 wt % Y_2O_3	R_{com} temperature	1000 °C
As received material	960 ± 101	603 ± 39
Corroded at 1000 °C, 50 h	644 ± 182	
Corroded at 1100 °C, 50 h	586 ± 74	
Corroded at 1200 °C, 50 h	530 ± 41	
Corroded at 1300 °C 50 h	425 ± 36	424 ± 44

[a] Values given are means ± standard deviation.

Only the 1100 °C test data (Equation 9) gave good parabolic kinetics, presumably related to the formation of a relatively thin surface layer (5 μm), without significant effects of bubbling and cracking. Relationship 10 (1200 °C) shows a distinct logarithmic component. At 1300 °C (Equation 11), while the best fit is logarithmic, a fit with both parabolic and logarithmic components could also be possible. The clear logarithmic nature of the oxidation reaction in the air + 1 vol % SO_2 gas substantiates the argument that simple best fitting of the parabolic law, and ignoring other laws, is not always justified. Indeed, the limited "parabolic only" approach will often lead to the wrong inference being made as to the identification of the rate controlling mechanism. Processes that effectively reduce the cross-section for diffusional transport of oxygen, or elements from the grain boundary phase, will lead to deviations from parabolic kinetics as proposed by Käll *et al.* [14]. For the Si_3N_4 material used in this study, the logarithmic component is considered to be associated with changes occurring in the surface scale during the progress of the corrosion process. For example, devitrification of silica, reaction between particulate SiO_2 and melts, formation of complex Y-based silicates and sub-surface gas bubbling will cause deviations from parabolic, diffusion controlled processes.

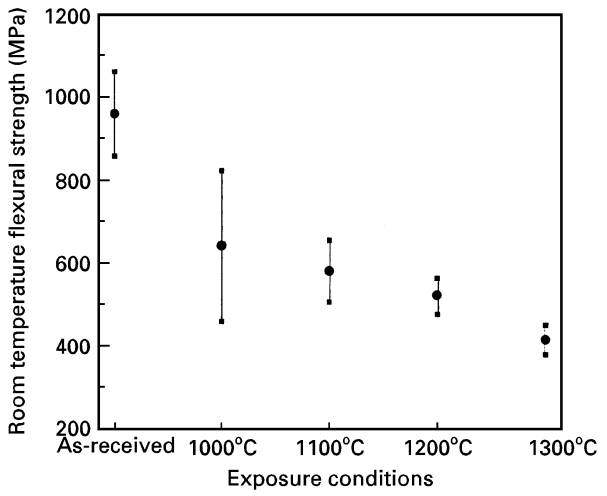

Figure 11 Room temperature flexural strength of specimens exposed in the combustion gas in the burner rig.

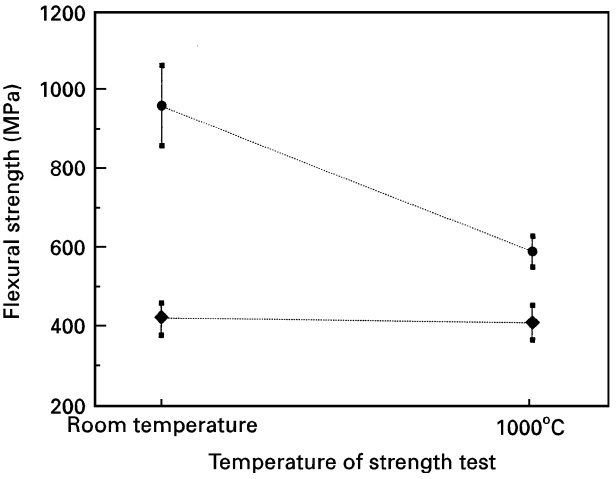

Figure 12 Comparison of the flexural strengths determined at room temperature and elevated temperature, (● as-received material; ◆ burner rig, 50 h at 1300 °C).

Comparing the material behaviour under oxidation in air and corrosion in the burner rig (Fig. 3), it can be hypothesized that corrosion in the presence of "basic" metal oxides (i.e. Na_2O) quickly leads to dissolution of potentially protective silicon dioxide surface films and liquid silicate formation, the presence of which permits an accelerated rate of transport that is manifested in a higher rate of corrosion. The observed corrosion kinetics depend on the silicate film composition, and thus viscosity, which is governed by the supply of metal cations (Al and Y from the grain boundary phase) and the presence of the salt and sulfur contaminants from the atmosphere. The formation of glassy silicate scales containing crystalline SiO_2 and $Y_2Si_2O_7$ during the oxidation of Si_3N_4, containing Y_2O_3 as the sintering aid, have previously been observed by several authors [4, 5, 15]. The effect of Na is to induce a rate of burner rig corrosion at 1000 °C similar to the rate of oxidation in air at 1200 °C.

The severe attack of Si_3N_4, and particularly of intergranular phases, causes the marked strength degradation due to the formation of defects in the surfaces of the test bars. The defects are mainly in the form of pits. While a large strength reduction was measured at 1000 °C on the as-produced material, the samples corroded at 1300 °C showed the same strength at room temperature and at 1000 °C. This demonstrates the importance of the annealing effect on the grain boundary phase, which crystallizes during high temperature corrosion testing, and is then more stable under the subsequent high temperature bend test. One contribution to the strength degradation has previously been attributed to the removal of surface stresses which derive from the specimen machining process [16, 17]. This contribution has been estimated to be of the order 200 MPa [18] on similar silicon nitride-based materials. In the assessment of the magnitude of the effect of corrosion damage on mechanical properties, it is necessary to take into account the above factors. However, owing to the limited amount of data obtained in this work, a firm conclusion as to the major cause of reduced strength cannot be deduced.

5. Conclusions

From relatively short time (50 h) exposures of a hot-pressed Si_3N_4 in a burner rig combustion atmosphere in the temperature range 1000 to 1300 °C, the following conclusions were drawn.

(a) The rate of surface reaction could be approximated to a parabolic law, although more detailed analysis of the weight change data showed a strong logarithmic component at the higher test temperatures ($\geqslant 1200$ °C).

(b) Using the parabolic approximation, an apparent activation energy of 387 kJ mol^{-1} was determined.

(c) Corrosion products formed on the surface of the ceramic were composed of continuous layers of silica, present in both glassy and crystalline (cristobalite) forms, as well as discrete particles of yttrium disilicate near the outer scale/gas interface.

(d) Strength is reduced by exposure at high temperature, but while the decrease after corrosion testing at, for example, 1300 °C was 56%, a contribution (probably around 20%) could also be attributed to the removal of surface stress.

Acknowledgements

The authors wish to acknowledge the contributions of A. Burke, P. Glaude and K. Schuster of Petten for their assistance throughout the course of this work and of Dr S. Guicciardi of Faenza for his helpful discussion on the mechanical properties results. This work was part of a collaborative project between CNR-IRTEC, Faenza, Italy and the Institute for Advanced Materials, JRC Petten, The Netherlands.

References

1. J. R. NICHOLLS and S. R. J. SAUNDERS, *High Temp. Technol.* **7** (1989) 193.
2. N. S. JACOBSON, *J. Amer. Ceram. Soc.* **76** (1993) 3.
3. G. B. DAVIES, T. M. HOLMES and O. J. GREGORY, *Adv. Ceram. Mater.* **3** (1988) 542.
4. G. N. BABINI, A. BELLOSI and P. VINCENZINI, *J. Mater. Sci.* **19** (1984) 1029.
5. A. BELLOSI, G. N. BABINI, H. LI-PING and F. XI-REN, *Mater. Chem. Phys.* **26** (1990) 21.
6. A. BELLOSI and G. N. BABINI, *Key Engng Mater.* **89–91** (1994) 117.
7. S. R. J. SAUNDERS and J. R. NICHOLLS, *High Temp. Technol.* **7** (1989) 232.
8. G. ERIKSSON, *Chem. Scripta* **8** (1975) 100.
9. JIS R 1609, Japanese Industrial Standard, "Testing methods for oxidation resistance of non-oxide high performance ceramics" (Japanese Standards Association, Japan, 1990).
10. A. BELLOSI and C. GALASSI, *Mater. Engng* **1** (1990) 949.
11. K. G. NICKEL, in "Corrosion of Advanced Ceramics: Measurement and Modelling", edited by K. G. Nickel, (Kluwer Academic Publishers, Dordrecht, 1994) pp. 59–71.
12. B. E. DEAL and A. S. GROVES, *J. Appl. Phys.* **36** (1965) 3770.
13. F. L. RILEY, in "Corrosion of Advanced Ceramics: Measurement and Modelling", edited by K. G. Nickel (Kluwer Academic Publishers, Dordrecht, 1994) pp. 85–96.
14. P. O. KÄLL, M. NYGREN and J. PERSSON, *ibid.* pp. 73–84.
15. J. B. VEYRET and M. BILLY, in Proceedings of the 1st European Ceramics Society Conference, ECERS-1, edited by R. A. Terpstra and R. Metselaar (Elsevier Applied Science, Barking, 1989) p. 512.
16. D. JOHNSON-WALLS, A. G. EVANS, D. B. MARSHALL and M. R. JAMES, *J. Amer. Ceram. Soc.* **69** (1986) 44.
17. A. G. EVANS, *Mater. Sci. Engng* **71** (1985) 3.
18. C. MELANDRI, S. TAGLIAFERRI, S. GUICCIARDI and G. ANDALÒ, *Ceram. Acta* **5** (1993) 73.

Received 20 April 1995
and accepted 17 September 1996